PHYSICAL AND MATHEMATICAL MODELLING OF SWIRLING FLOW TUNDISH

Q. F. HOU[1, 2], H. Y. WANG[1], Q. YUE[1], Z.S. ZOU[1] and A.B. YU[2]

[1] School of Materials and Metallurgy, Northeastern University, Shenyang, 110004, China
[2] Centre for Simulation and Modelling of Particulate Systems, School of Materials Science and Engineering, University of New South Wales, Sydney, NSW 2052, Australia

ABSTRACT

A new swirling flow tundish (SFT) has recently been developed through forming swirling flow to enhance inclusion removal from steel for high quality slab casting. This is achieved by guiding liquid steel into the tundish through the tangential inlet of a cylindrical swirling chamber (SC). To understand the fundamentals, physical and mathematical modellings have been conducted in this work. Physical modelling is carried out with the utilization of a 1:2.5 scale model. The internal flow is measured by digital particle image velocimetry. Numerical modelling is carried out in line with the physical modelling to examine details of the flow pattern and rotational effect caused by the SC. The trajectories of non-metallic inclusion particles are also studied using discrete phase model within the commercial CFD package environment, FLUENT. The mathematical model proposed is validated by comparing the predicted and measured residence time distributions and velocity fields. Examinations of the trajectories of inclusion particles suggest that inclusion removal capacity of the SFT is higher than a tundish with turbulence inhibitor (TI). From the separation ratio results, it can be seen that SFT has higher ability to remove small inclusion particles than a tundish with TI, which is significant especially in production of high-quality steel.

NOMENCLATURE

C Concentration of tracer, kg/m^3
D_e Effective turbulent mass diffusivity, m^2/s
D_{sc} Diameter of swirling chamber, mm
H Height of tundish, mm
H_{sc} Height of swirling chamber, mm
k Turbulent kinetic energy, J/kg
L_1 Length of top tundish, mm
L_2 Length of bottom tundish, mm
p Pressure, Pa
Q Inlet flowrate, Nm^3/h
R Radius of inclusion
Rt Rotational similarity criterion
u_i Velocity in the x_i direction, m/s
W_1 Width of top tundish, mm
W_2 Width of bottom tundish, mm
x_i Cartesian coordinates vector
Φ Diameter of inlet, mm
ε Dissipation rate of kinetic energy, m^2/s^3
ρ Density, kg/m^3
μ Molecular viscosity of fluid, Pa·s
μ_t Turbulent viscosity of fluid, Pa·s
μ_{eff} Effective viscosity of fluid, Pa·s
ω Rotational speed, rpm
subscript
inc   Inclusion
m   Model
p   Real unit
st   Steel
w   Water

INTRODUCTION

High steel quality, energy-saving and cost-saving, together with environmental friendliness, are key issues in modern metallurgical industry. In traditional steelmaking, a tundish acts as a reservoir and distributor settled between ladle and caster. Recently, it also plays an important role of producing clean liquid steel by removing some unwanted inclusions. For these purposes, various kinds of flow control devices, such as dam, weir, turbulence inhibitor (TI) and stopper, have been developed in recent decades (Mazumdar and Guthrie, 1999). In addition, some new methods have also been proposed in continuous casting process, e.g. plasma heating for maintaining appropriate casting steel temperature (Barreto-Sandoval, et al., 1996) and gas bubbling curtains to enhance inclusion removal by adhesion (Ramos-Banderas, et al., 2003). In addition to those renovations, two typical kinds of tundishes are developed, centrifugal flow tundish (CFT) (Miki, et al., 1996) and swirling flow tundish (SFT) (Zou, et al., 2004). CFT, developed by Kawasaki Steel (now JFE Steel Corporation), is a special one for inclusion removal. This kind of tundish utilizes external electromagnetic force to rotate molten steel in a cylindrical tundish and to enhance inclusion removal by centrifugal force field. However, external electromagnetic apparatus must be used in this kind of tundish, which increases the cost of production. Consequently, a huge amount of electricity is also consumed. It is neither environmentally friendly nor energy-saving. Despite the shortcomings of CFT, it was used in commercial production of high-quality stainless steel slabs after industrial tests at Chiba. However, the effects of CFT for inclusion removal have been verified, since the rotational field can enhance the removal of inclusion at 40~50rpm. Based on the idea of CFT, SFT is developed recently with a swirling chamber (SC) to produce rotational motion without extra energy consumption. While SFT can achieve similar metallurgical effects, external apparatus is no longer required to produce the centrifugal force field. In fact, the gravity force of steel flow can be harnessed during continuous casting. By guiding the steel into a cylindrical chamber through its tangential inlet, the translational energy of steel liquid can be

transformed into a rotational one. Hence, a rotational flow field is formed in the chamber. In this way, SFT can fulfil the roles of both turbulence inhibition and inclusion removal. The variation of flow patterns in SC has been examined (Hou and Zou, 2005a) in detail by commercial software package. And the influences of parameters of cylindrical SC on the whole flow field of SFT have also been studied by in-house code (Hou and Zou, 2005b).

In this work, cold physical and mathematical models are developed for one strand slab SFT. The mathematical model is then validated by both overall residence time distribution (RTD) curves and more specific flow field measurements by digital particle image velocimetry (DPIV). Furthermore, the separation ratios of inclusion between SFT and a tundish with TI are compared. Based on these comparison and analysis of trajectories of inclusion particles, the positions of flow control devices are adjusted to improve the separation ratio in SFT.

MODEL DESCRIPTION

Main Dimensions of Model

Main features of the mathematical and cold physical models are shown in Fig. 1 and the relevant dimensions are given in Table 1. The coordinate system is shown in Fig.1 for following discussion too.
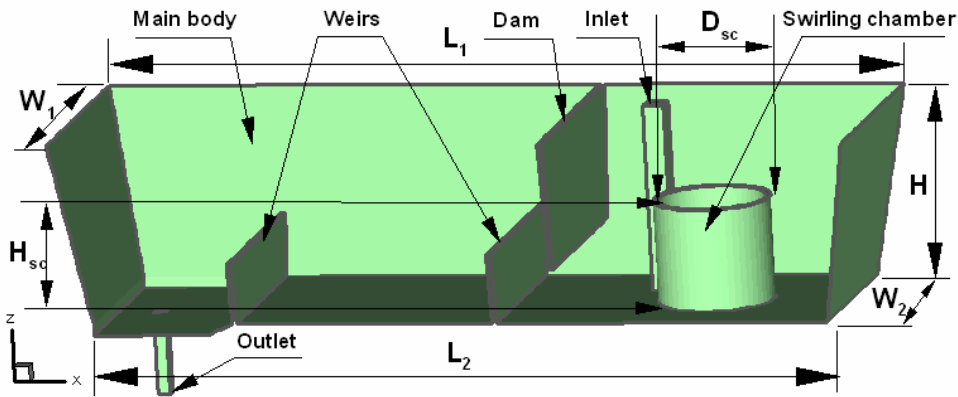
Figure 1: Swirling flow tundish configuration and coordinate system

Dimensions	L_1	L_2	W_1	W_2	H	H_{sc}	D_{sc}	Φ
Values, mm	1800	1665	610	480	420	90~260	170~320	30

Table 1: Dimensions of mathematical and physical models

Numerical Method

All mathematical simulations are carried out within commercial software package environment, FLUENT. The governing equations solved for the flow fields are the standard conservation equations of mass and momentum in the mathematical simulations. The equation for RTD is a normal species transportation equation. For trajectories of the inclusion, discrete phase model (DPM) is employed with revised wall boundary conditions. The free surface and tundish walls have different boundary conditions (such as reflection and entrapment) for droplets/solid inclusion particles. Taking the range of inclusion particles' diameter (Chevrier and Cramb, 2005) and the shapes for different types of inclusions (Beskow, et al., 2002) into consideration, the boundaries and drag law for particles are then revised by user defined function (UDF) and shape correction coefficient. During trajectory simulations, Stokes-Cunningham drag law is employed with Cunningham correction. Inclusions sometimes could be liquid phase. It is difficult to set the correction coefficient (Haider and Levenspiel, 1989) exactly since droplets can move and deform continuously. While Sinha and Sahai (1993) set both top free face and walls as trap boundary, Lopez-Ramirez et al. (2001) did not illustrate the boundary conditions for inclusion. Zhang, et al. (2000) divided the tundish into two kinds of separate zones. The walls are set as

reflection boundary in this work for comparison of separation ratios of inclusion in SFT and a tundish with TI. Although most of the reports indicate that the free surface is a trap boundary, there is a possibility of re-entrainment (Bouris and Bergeles, 1998) to be considered.

Given that the fluid is incompressible (i.e. the density of water is constant at 998.2kg/m^3), the modified conservation equations take the following forms:

Continuity equation:

$$\frac{\partial(u_i)}{\partial x_i} = 0 \tag{1}$$

Momentum equation:

$$\rho u_j \frac{\partial u_i}{\partial x_j} = -\frac{\partial p}{\partial x_i} + \frac{\partial}{\partial x_j}\left[\mu_{eff}\left\{\frac{\partial u_i}{\partial x_j} + \frac{\partial u_j}{\partial x_i}\right\}\right] \tag{2}$$

Turbulent kinetic energy equation:

$$\frac{\partial(\rho u_j k)}{\partial x_j} = \frac{\partial}{\partial x_j}\left(\frac{\mu_{eff}}{\sigma_k} \times \frac{\partial k}{\partial x_j}\right) + G - \rho\varepsilon \quad (3)$$

Turbulent kinetic energy dissipation rate equation:

$$\frac{\partial(\rho u_j \varepsilon)}{\partial x_j} = \frac{\partial}{\partial x_j}\left(\frac{\mu_{eff}}{\sigma_\varepsilon} \times \frac{\partial \varepsilon}{\partial x_j}\right) + \frac{(C_1 G\varepsilon - C_2 \rho\varepsilon^2)}{k} \quad (4)$$

Species transport equation:

$$\frac{\partial C}{\partial t} + \frac{\partial}{\partial x_i}(u_i C) = \frac{\partial}{\partial x_i}(D_e \frac{\partial C}{\partial x_i}) \quad (5)$$

where,

$$G = \mu_t \frac{\partial u_j}{\partial x_i}(\frac{\partial u_i}{\partial x_j} + \frac{\partial u_j}{\partial x_i}) \quad (6)$$

effective viscosity:

$$\mu_{eff} = \mu + \mu_t = \mu + \rho C_\mu \frac{k^2}{\varepsilon} \quad (7)$$

Effective mass-diffusion coefficient, which depends on the fluid flow field (He and Sahai, 1987), can be calculated through:

$$\frac{\mu_{eff}}{\rho D_e} \approx 1 \quad (8)$$

The constants (Launder and Spalding, 1974) in the k-ε two equations turbulence model are $C_1 = 1.44$, $C_2 = 1.92$, $C_\mu = 0.09$, $\sigma_k = 1.0$, and $\sigma_\varepsilon = 1.3$.

Boundary conditions for flow field calculations are similar to those used by other researchers (Kumar et al., 2004) for steady 3D isothermal flow in tundish.

Physical Model

The physical model is created according to a real unit of an industrial tundish under similarity principle. The selected physical scale factor λ is 1:2.5. The structure of water model for experiments is shown in Fig. 2. It is made of transparent acrylic glass. Water model experiments are carried out at three flowrates $Q_{1,2,3} = 2, 2.5, 3$ Nm^3/h.

Figure 2: Physical model of SFT

RESULTS AND DISCUSSION

Model Validation

RTD curves are the most common method to estimate the particle separation and to analyse flow conditions. The experimental results are obtained by pulse tracer addition technique. The predicted results are calculated out by two-step simulation. The first step is to calculate the steady flow field. The second step is to solve the species transport equation using unsteady solver based on the steady flow results of the first step. Figure 3 shows the comparison of experimetral and predicted results with the same conditions (Q_2, D_2 and H_5).
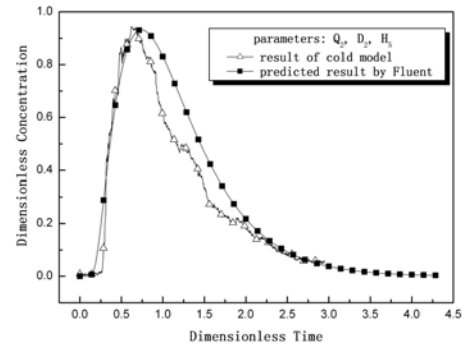
Figure 3: Comparison of RTD curves

The comparison of the flow fields is also carried out and given in Fig. 4. The scale and distribution of velocity field are similar. The measured result is obtained using DPIV with a kind of particle with slightly higher density than water, 1050kg/m^3. The tracer particle diameter is in the range of 1 to 5μm.
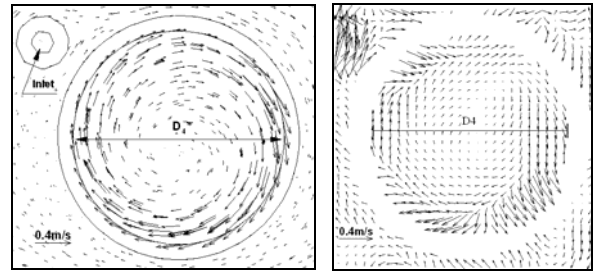
a) Predicted result   b) Measured result

Figure 4: Comparison between predicted and measured velocity fields

Asymmetrical flow field

The asymmetrical flow field can be seen in Fig. 5 in the impact zone (the area below the inlet) and in areas behind the dam and weirs. It is a horizontal xy-section at height of z=200mm to the bottom of tundish. The rotational and large velocity flows are mostly confined in SC domain. The slow and uniform flow behind the wall is beneficial for flotation of inclusion to the top slag-steel interface, which is the mainly mechanism for inclusion removal.
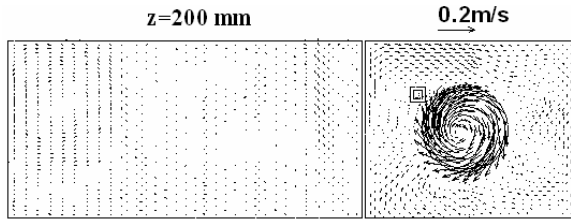
Figure 5: Asymmetrical flow field (Q_1, H_4 and D_3)

Influence of swirling chamber geometry

For the study of the influence of SC geometrical parameters on rotational speed, a series of cylindrical SCs are employed and their dimensions are given in Table 2.

D_{sc}	D_1	D_2	D_3	D_4	D_5
mm	170	200	240	280	320
H_{sc}	H_1	H_2	H_3	H_4	H_5
mm	90	140	180	220	260

Table 2: Swirling chamber dimensions

Swirling chamber diameter has great influence on axial velocity distribution in SC (shown in Fig. 6). The velocity distributions have negative velocity in the centre and positive velocity near the wall of SC for both two diameters (D_3 and D_5). With the smaller diameter (D_3), the axial velocity distribution in x-direction is similar to that in y-direction. However, with the larger diameter (D_5), these distributions are different. In the range of -0.12~0m, the value of velocity in x-direction is less than that in y-direction. In the range of 0~0.12m, there is a reverse trend.

Through the results of simulations and measurements, it is shown that the maximum rotational speed obtained in SC is ω=70rpm, which is comparable to the speed of 40~50rpm obtained from CFT (Miki, et al., 1996). According to the similarity criterion Rt (Rt = $l^3 Q^{-1} \omega$), the rotational speed that can be maximally achieved is 44rpm in real unit. The variation trend of rotational speed with diameter and height of SC can be found in another publication (Zou, et al., 2004).
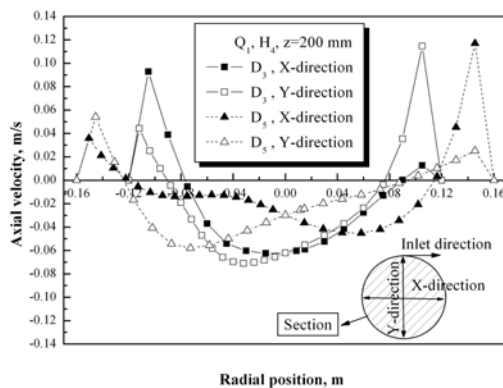
Figure 6: Influence of SC parameters on velocity distribution

Pathlines of flow field

Pathlines of fluid in SFT and the tundish with TI are given in Fig. 7. It shows that pathlines in SFT are much more complicated than those of the tundish with TI in the impact zone. It should be point out that some pathlines of SFT that go out of SC go back into SC again. Since the pathlines become longer in SFT, the residence of fluid will be extended actually to some degree.

a) SFT

b) Tundish with TI
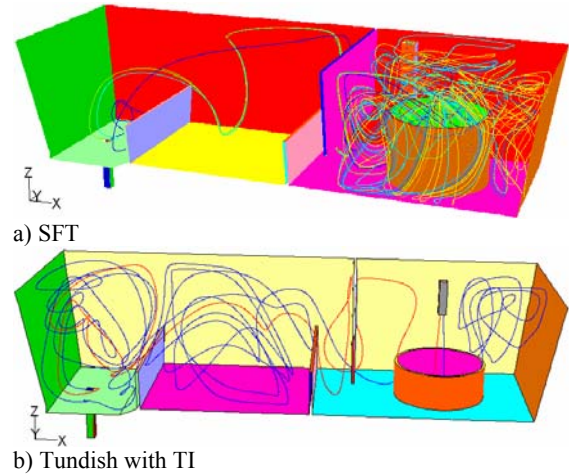
Figure 7: Pathlines of flow field

Similarity analysis of inclusion particle

The non-metallic inclusion particles are lighter than molten steel in real unit and, thus, will rise up to the slag-steel interface. Since the response time of inclusion in tundish is extremely short, the flotation velocity of inclusions can be determined as Stokes' velocity.

Unfortunately, in physical modelling, it is difficult to create particles with identical density and diameter to the real situation. Therefore, it is necessary to analyse the similarity of particles in model and real tundishes. Sahai and Emi (1996) have analysed the similarity of particles. Assuming that the kinematic viscosity of water at room temperature is the same as that of steel at 1,873k, one obtains

$$\frac{R_{inc,m}^2}{R_{inc,p}^2} \cdot \frac{1 - \rho_{inc,m}/\rho_w}{1 - \rho_{inc,p}/\rho_{st}} = \sqrt{\lambda} \qquad (9)$$

For mathematical modelling, $R_{inc,\,m}$ can be chosen to be the same as $R_{inc,\,p}$. Consequently, ρ can be calculated as 640 kg/m³ for the inclusion density of 3,000kg/m³ in real condition according to the similarity criterion (Equation 9).

In fact, a similarity criterion can also be obtained by dimensional analysis. Taking kinematic viscosity μ, density ρ, the difference of density ($\rho_l - \rho_{inc}$), radius r, relative velocity u, and gravitational acceleration g into consideration, three dimensionless groups can be formed, Re^{-1}, Fr^{-1}, and $(\rho_l - \rho_s)/\rho_l$. According to Buckingham's Π Theorem, the group of $Re \cdot Fr^{-1} \cdot (\rho_l - \rho_s)/\rho_l$ is actually the same as the analysis result of Sahai and Emi's.

Trajectories of inclusion particles

Different densities of inclusion were used in the literatures, e.g. 3,500kg/m^3 for spherical particles and 5,000kg/m^3 for clusters (Lopez-Ramirez et al., 2001), 2,700 kg/m^3 for spherical inclusions (Sinha and Sahai, 1993). Three densities are considered in this work for mathematical model simulation (400, 500, 600kg/m^3) to examine the influence of density on separation ratio of inclusion.

a) SC (H$_4$, D$_3$, Q$_1$, 20μm, 500kg/m^3)

b) TI (Q$_1$, 20μm, 500kg/m^3)
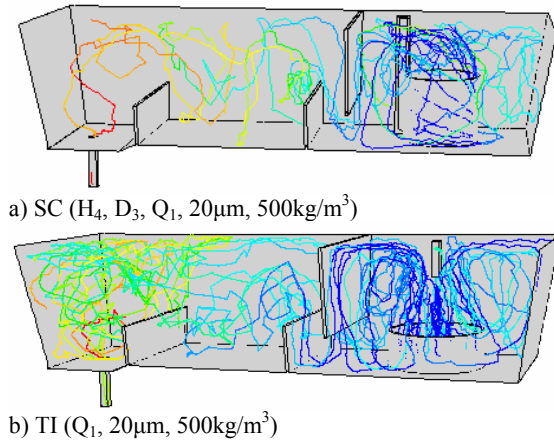
Figure 8: Trajectories of particles in tundishes

The injection of a particle is set. The original injection position is on the inlet surface. The injected particles are set with different diameters and densities. 2,000 particles are released each time and their trajectories are calculated out with discrete random walk model. Each injection condition is repeated five times and then the total separation ratios are calculated. Twenty representative trajectories of inclusion particles in SFT and a tundish with TI are shown in Fig. 8. It can be seen that the trajectories for the same kind of inclusion particle are different. In the tundish with SC, most particles have longer trajectories in the impact zone than those in the tundish with TI. This can enhance the removal of inclusion to slag-steel interface. Moreover, in the zone above the outlet, it can be seen that inclusion particles in the tundish with TI have greater possibility to go into mold than those in the tundish with SC.

Comparison of removal possibility

The influence of density on separation ratio is given in Fig. 9. It can be seen that the differences of density have a minor influence on separation ratio within the density range of 400~600kg/m^3. Moreover, according to the weight of inclusion distribution (shown in Fig. 10) from experimental samples, particles that are larger than 75μm have little significance and can be neglected during simulation process.
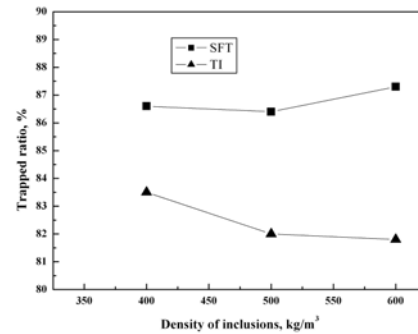
Figure 9: Relationships of removal ratio and density of inclusion particles

For larger diameters of particle (50μm), the separation ratio of tundish with TI is higher than that of SFT. The reason for this is the short distance between the dam and the first weir or between dam and SC which can be seen from the trajectories shown in Fig. 11 (a, b). Because of these narrow spaces, the upward flow is very quick and it can be reflected instantly downward. Consequently, the entrainment possibility of inclusion particles to slag-steel interface is decreased for inclusion particles. The SFT has been revised to alleviate this phenomenon. Both of the distances between the dam and the first weir and between the weir and SC have been extended 100mm in one simulation. It can be seen from Fig. 11 (c) that the strong upward flow is weakened. As a result, the separation ratios of inclusions are improved as shown in Table 3, particularly for the 20μm diameter particles.
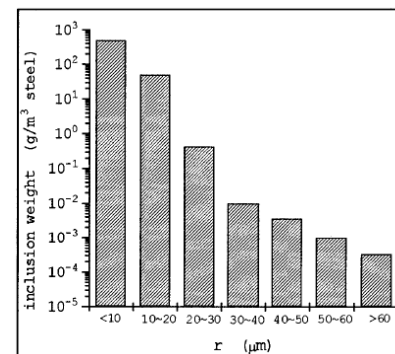
Figure 10: The size distribution of inclusion in weight extracted from steel by Slimes method (Zhang, et al., 2000)

Tundish \ Diameter, μm	20	50	60	80
TI, %	82.00	94.95	97.27	99.10
SFT, %	86.40	92.30	94.09	97.67
Adjusted SFT, %	89.85	93.68	95.19	97.95

Table 3: Separation ratio in different kinds of tundish (ρ=500kg/m^3)

a) SFT

b) TI

c) Adjusted SFT
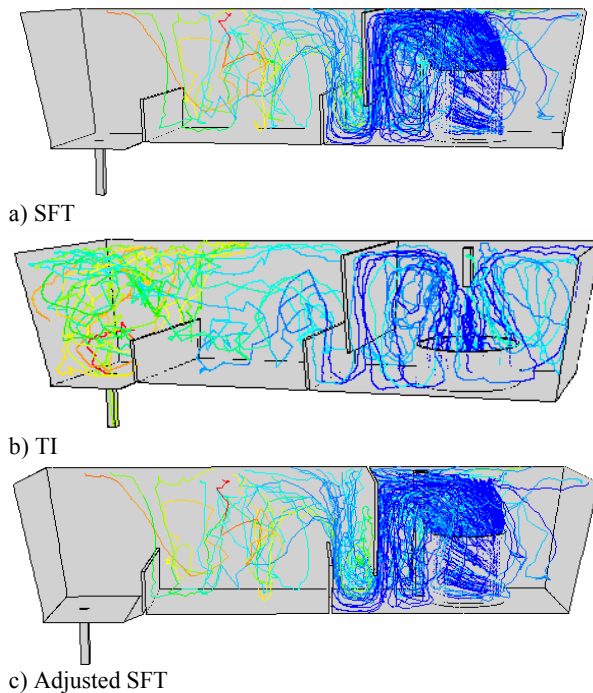
Figure 11: Trajectories of particles

It should be pointed out here that the original positions of flow control devices were optimized for tundish with TI. However, the results show that they are no more suitable for SFT. For different design of flow control schemes, their positions should be relocated for optimum operation.

CONCLUSIONS

A new swirling flow tundish has been developed and modelled by physical and mathematical methods. The numerical model is validated by measured RTD curves and flow field respectively. The flow field, the movement and separation of inclusions are examined too. The conclusion can be drawn as follows.

1. Small inclusions have higher probability of flotation to slag-steel interface in SFT than the tundish with TI. The separation ratios show that SFT has a greater ability to remove small inclusion (such as 20μm) than the tundish with TI.

2. For different designs of tundish, the positions of all flow control devices should be relocated for optimum metallurgical effects.

ACKNOWLEDGEMENT

REFERENCES

D. Mazumdar and R. I. L. Guthrie, (1999), Physical and mathematical modelling of continuous casting tundish systems, ISIJ Int., 39, 524.

J. d. J. Barreto-Sandoval, A. W. D. Hills, M. A. Barron-Meza and R. D. Morales, (1996), Physical modelling of tundish plasma heating and its mathematical interpretation, ISIJ Int., 36, 1174.

A. Ramos-Banderas, R. D. Morales, L. Garcia-Demedices and M. Diaz-Cruz, (2003), Mathematical simulation and modeling of steel flow with gas bubbling in trough type tundishes, ISIJ Int., 43, 653.

Y. Miki, S. Ogura and T. Fujii, (1996), Separation of inclusions from molten steel in a tundish by use of a rotating electromagnetic field, Kawasaki Steel Technical Report, 67.

Z. Zou, Q. Hou, S. Kuang, et al.: "Feasibility Study of a Swirling Flow Tundish", 2nd international conference on process development in iron and steelmaking, Luleå Sweden, 2004.

Q. F. Hou and Z. S. Zou, (2005a), Study on fluid flow in swirling chamber of swirling flow tundish, Kang T'ieh/Iron and Steel (Peking), 40, 33.

Q. Hou and Z. Zou, (2005b), Numerical and physical simulation of flow patterns in a swirling flow tundish, Steel Res. Int., 76, 726.

V. Chevrier and A. W. Cramb, (2005), Observation and measurement of bubble separation at liquid steel-slag interfaces, Scand. J. Metall., 34, 89.

K. Beskow, J. Jia, C. H. P. Lupis and S. C. Du, (2002), Chemical characteristics of inclusions formed at various stages during the ladle treatment of steel, Ironmaking & Steelmaking, 29, 427.

A. Haider and O. Levenspiel, (1989), Drag coefficient and terminal velocity of spherical and nonspherical particles, Powder Technology, 58, 63.

A. K. Sinha and Y. Sahai, (1993), Mathematical modeling of inclusion transport and removal in continuous casting tundishes, ISIJ Int., 33, 556.

S. Lopez-Ramirez, J. D. J. Barreto, J. Palafox-Ramos, R. D. Morales and D. Zacharias, (2001), Modeling study of the influence of turbulence inhibitors on the molten steel flow, tracer dispersion, and inclusion trajectories in tundishes, Metallurgical and Materials Transactions B: Process Metallurgy and Materials Processing Science, 32, 615.

L. F. Zhang, S. Taniguchi and K. K. Cai, (2000), Fluid flow and inclusion removal in continuous casting tundish, Metall. Mater. Trans. B-Proc. Metall. Mater. Proc. Sci., 31, 253.

D. Bouris and G. Bergeles, (1998), Investigation of inclusion re-entrainment from the steel-slag interface, Metallurgical and Materials Transactions B: Process Metallurgy and Materials Processing Science, 29, 641.

Y. He and Y. Sahai, (1987), The Effect of Tundish Wall Inclination on the Fluid-Flow and Mixing - a Modeling Study, Metallurgical Transactions B-Process Metallurgy, 18, 81.

B. E. Launder and D. B. Spalding, (1974), The numerical computation of turbulent flows, Computer Methods in Applied Mechanics and Engineering, 3, 269.

A. Kumar, S. C. Koria and D. Mazumdar, (2004), An assessment of fluid flow modelling and residence time distribution phenomena in steelmaking tundish systems, ISIJ Int., 44, 1334.

Y. Sahai and T. Emi, (1996), Criteria for water modeling of melt flow and inclusion removal in continuous casting tundishes, ISIJ Int., 36, 1166.